Physical Modeling and Template Design for UWB Channels with Per-Path Distortion

Li Ma*, Alexandra Duel-Hallen* and Hans Hallen^
Department of *Electrical and Computer Engineering, ^Physics
North Carolina State University
Raleigh, NC 27695 U.S.A.
lma4@ncsu.edu, Sasha@ncsu.edu, Hans_Hallen@ncsu.edu

ABSTRACT

Recent experimental and physical modeling studies demonstrate that, as opposed to systems with smaller bandwidth, the Ultra-Wideband (UWB) channel exhibits frequency-dependent distortion of individual multipath components. This per-path distortion is particularly significant in outdoor UWB applications, where line-of-sight (LOS) or non-distorted reflected signals might not be available at the receiver (for example, in a canyon-like street). In these cases, the dominant propagation mechanisms involve shadowing (diffraction) and reflection by small objects (e.g. signs or a lamp-posts). In this paper, a physical model is developed to investigate the position-dependent distortion of the UWB pulse. The results indicate that both the shadowed pulse and the reflected pulse (by small objects with dimensions bounded by the wavelengths present in the signal) are distorted. Design of optimal and suboptimal templates for the correlation receiver are investigated. The UWB pulses that accommodate robust template choice given by the transmit pulse shape for all propagation conditions and satisfy the FCC spectral mask for outdoor channels are identified. Finally, we analyze the frequency-dependent propagation gain of the UWB channels in various outdoor conditions. This knowledge quantifies the potential benefits of adapting the transmitted signal to the dominant propagation mechanism.

I. INTRODUCTION

UWB communications has the potential to provide low-cost and high-speed service, and has attracted increasing interest since the release of FCC spectral masks in 2002 [1]. These masks allow the use of 0~0.96 GHz and 3.1~10.6 GHz bands on an unlicensed basis subject to certain restrictions on the signal power spectrum density (PSD). Specifically, UWB technology is defined as any wireless transmission scheme that possesses a fractional bandwidth $W/f_c \geq 20\%$, where W is the transmission bandwidth and f_c is the center frequency, or an absolute -10 dB bandwidth which exceeds 500 MHz [1]. Since the early 90's, the vast majority of UWB research has focused on impulse radio techniques that employ transmission of very short pulses. A unique advantage of impulse radio is its potentially low implementation complexity [2]. Time-Hopping Pulse Position Modulation (TH-PPM) [3] and the Direct-Sequence UWB (DS-UWB) [4, 5] are examples of impulse radio methods. Recently, multi-band Orthogonal Frequency Division Multiplexing (MB-OFDM) [6] method that does not utilize UWB pulses has emerged as strong candidate for the Wireless Personal Area Network (WPAN) standard [7]. While we concentrate on impulse radio UWB system in this paper, our results have direct impact on techniques investigated in this recent proposal.

Due to the exceptionally wide bandwidth of the UWB channel, the frequency independence assumption implied in systems with smaller bandwidth for the impulse response of the individual multipath components does not always hold. While the model adopted in [3,8] does not address this issue (with the exception of the antenna gains), several experimental and physical modeling studies demonstrate that, the UWB channel can exhibit frequency-dependent per-path distortion [9, 10] and this feature was incorporated in the IEEE 802.15.4a model [11]. In this paper, we focus on outdoor UWB applications, where per-path distortion can occur due to shadowing (diffraction), reflections from small objects, rain, trees, etc. While diffracted signals are typically weaker than LOS or reflected signals (for sufficiently large reflector sizes), they can be dominant in certain outdoor environments, e.g. a canyon-like street or when the antenna is located behind a hill from the transmitter, where the signal arrives at the receiver only after it has been diffracted around an intervening object (and/or after reflection by a small reflector). The power loss in the shadow is often lower than the loss caused by building penetration, thus resulting in more reliable reception in some outdoor environments [12]. The strength of the diffracted signal depends strongly on the wavelength of the signal with larger loss for higher frequencies.

Physics-based studies on UWB pulse distortion have been reported in [9, 13], in which the diffracted pulse is derived directly from expressions of the Uniform Theory of Diffraction (UTD) and Geometry Theory of Diffraction (GTD). The physical model described in this paper is based on a Fresnel diffraction augmentation of the method of images [14-16], and provides a more accurate description of how the strength and shape of the received pulse changes with position in given local environment. In this paper, we utilize our physical model to study the channel distortion

This research was supported by NSF grant CCR-0312294 and ARO grant W911NF-05-1-0311.

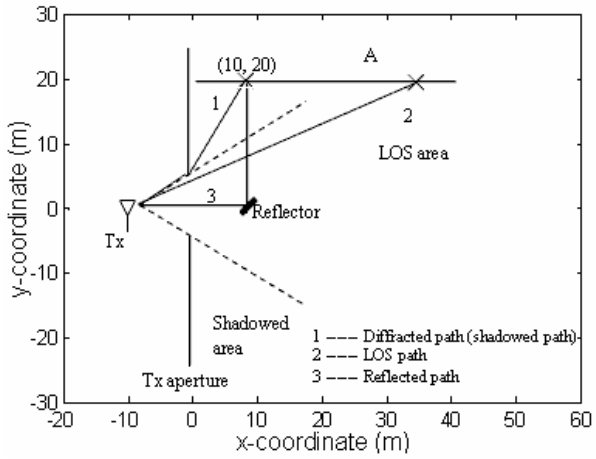

Figure 1. A simple geometry for the UWB physical model.

for several families of pulses that are widely employed in the UWB literature [3, 17-20]. Per-path distortion requires careful choice of template for the correlation receiver [3, 9, 10]. We explore several low complexity templates and identify transmit pulses that result in reliable performance when the transmit pulse shape is employed as template for diverse propagation mechanisms, thus greatly simplifying the receiver design. These pulses satisfy the FCC spectral mask for outdoor channels [1]. Finally, we analyze and compare the propagation gains of pulses transmitted in two disjoint bands of the spectral mask, and discuss the impact of this study on possible adaptive transmission methods.

This paper is organized as follows. Section II describes our physical model. In section III, we discuss the effect of distortion on several families of pulses and identify pulses that fit the FCC spectral mask and perform well with simple and robust correlation templates. We compute the frequency-dependent propagation gain for varying channel conditions using pulses that occupy disjoint bands of the spectral mask, and discuss implications on design of adaptive transmission methods for UWB channels in Section IV.

II. UWB Physical Channel Model and System Model

A. Physical Model

We utilize a physical UWB channel model based on the Fresnel diffraction theory combined with the method of images [14-16]. This modeling approach is based on principles similar to those employed for modeling frequency selective fading channels in [14]. Geometry that specifies the parameters associated with dominant objects in the environment, e.g. the positions, angles, sizes, shapes (spherical or flat), the reflectivities, etc., serves as the input to the model. The physical model produces the frequency response of the simulated UWB channel. We obtain the

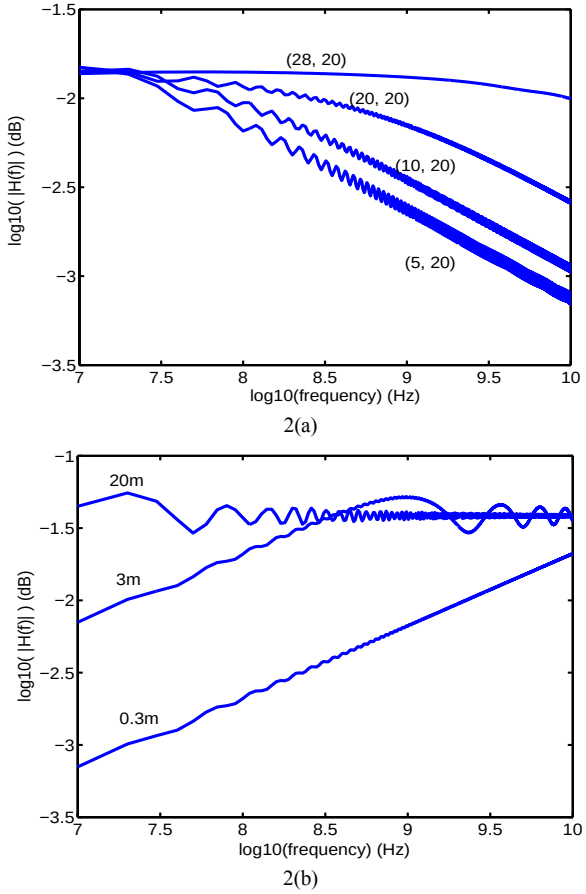

Figure 2. Amplitude of Frequency responses of distorted UWB channels, (a) Diffraction path at different positions in Fig. 1, (b) Reflection (path 3) for different reflector sizes, coordinate (10, 20) in Fig. 1.

received pulse by computing Inverse Fourier Transform (IFT) of the product of the Fourier Transform (FT) of the transmitted pulse with the modeled channel frequency response. Fig. 1 shows a simple example of input geometry that contains only one reflector. An aperture for the transmitter is used to model regions in LOS and those shadowed from the transmitter. Three propagation mechanisms, the LOS (path 2), diffraction (path 1) and reflection (path 3) are shown in the figure.

While the LOS channel does not distort the transmitted pulse [21], the amplitudes of the frequency responses of the diffracted and reflected paths (when the size of the reflector is on the order of the wavelength or less) shown in Fig. 2 indicate that significant distortion is present over the frequency range of the UWB channel. We note that these responses are calculated from the ratio of the electric field at the receiver antenna to the electric field 1 m from the transmitter [21], and do not include the response of either antenna. As illustrated in Fig. 2(a), high frequency components are strongly attenuated in diffracted channels. We observed that the slope of the amplitude of the channel transfer function resembles that of $H(f)=1/\sqrt{f}$ for deep

shadowing, while the integrator with response *1/f* provides satisfying intuitive explanation for the distortion associated with diffracted channels. The latter two responses were reported for diffracted channels in [13, 22], with the $1/\sqrt{f}$ representing the most common diffraction case in outdoor applications - diffraction by a wall corner of a building. As the receiver moves from the diffracted region to the LOS region, the shape of the frequency response becomes gradually flatter as shown in Fig. 2(a). For the reflection by small reflector (Fig. 2(b)), the low frequencies experience great loss, and the slope of the response is modeled well by that of $H(f)=\sqrt{f}$, while the derivative $H(f)=f$ is a simple approximation to this channel. As the reflector size increases, the channel response in Fig. 2(b) approaches the ideal flat channel response. When the reflector size is 20m or greater, the received and the transmit pulses are indistinguishable. For all path responses, the phase response is approximately linear, with its derivative representing the path delay of the corresponding multipath component in the received signal.

B. System model and receiver signal processing

The multipath UWB channel impulse response can be modeled as $h(t) = \sum_{k=1}^{L} h_k(t-\tau_k)$,where $h_k(t)$ is the impulse response that incorporates the channel gain (but not the delay) and τ_k is the delay, respectively, of the k^{th} path (i.e., multipath component), and L is the total number of paths [18]. All channel parameters vary slowly, but the time dependency is suppressed for simplicity of notation. Assume transmit pulse waveform $p_t(t)$. While we do not directly model the antenna effects [8, 10, 11], we assume that the electronic pulse shape is designed to correct for the transmit antenna frequency-dependence, and $p_t(t)$ is the resulting transmitted signal. In practice, the receiver template should include an additional filter that accounts for the receive antenna distortion. Then the received signal can be expressed as $r(t)= \sum_{k=1}^{L} p_r^{(k)}(t-\tau_k) + n(t)$, where $p_r^{(k)}(t) = h_k(t) * p_t(t)$ represents the received pulse waveform associated with the k^{th} path, $n(t)$ is zero-mean, Additive White Gaussian Noise (AWGN) random process with double-sided power spectrum density $N_0/2$, and '*' denotes convolution. In typical UWB channels, the received signal contains many resolvable multipath components [3]. Each of these components corresponds to a path (or a superposition of several paths), affected by some propagation mechanism, and can correspond to one of the paths illustrated in Fig. 1. The transmitted signal is detected by collecting the energy associated with dominant (strongest) multipath components using the RAKE receiver [3, 8]. Channel response of each of these paths could affect both the receiver correlation template employed by the receiver and the received signal-to-noise ratio (SNR). For simplicity, we focus on single-path case, i.e. L=1, in this paper. Then the received signal reduces to

$$r(t) = p_r(t-\tau) + n(t), \qquad (1)$$

where $p_r(t)$ is the received pulse and τ is the delay. The correlation receiver is employed at the detector [3, 8]: $\int_{-\infty}^{\infty} r(t)v(t-\hat{\tau})dt$, where $v(t-\hat{\tau})$ is the normalized (unit energy) correlation template delayed by $\hat{\tau}$. Denote the energy of the received pulse $E_r = \int_{-\infty}^{\infty} p_r^2(t)dt$. We assume that the peak of the cross-correlation between the received pulse and the template

$$\rho = \int_{-\infty}^{\infty} p_r(t-\tau)\, v(t-\hat{\tau})dt \Big/ \sqrt{E_r} \qquad (2)$$

is achieved at $\hat{\tau}$. In practice, finite integration window is employed when calculating the cross-correlation. Define the $SNR_{out} = \frac{\rho^2 E_r}{N_0}$. The parameter ρ (2), plays a key role in the performance of the correlation detector. When per-path distortion is absent, the optimum template is the normalized transmit pulse $p_t(t)$, while the optimum choice of the template for any received pulse is $v(t)=p_r(t)/\sqrt{E_r}$, resulting in the maximized value of $\rho = 1$. However, if the template is not matched to the channel response, $\rho < 1$, resulting in reduced energy capture [10]. For example, to keep the dB loss (SNR_{out} reduction) caused by pulse distortion within 1dB, the value of ρ must be above 0.89. This loss is defined in terms of the SNR capture:

$$SNR_c = \rho^2 \text{ (dB)}. \qquad (3)$$

We discuss template design for impulse radio systems with per-path distortion in the next Section.

III. TEMPLATE DESIGN FOR CHANNELS WITH DISTORTION

Gaussian monocycles are frequently adopted as UWB pulses [3, 17]. The n^{th} order Gaussian monocycle is defined as the n^{th} derivative of the basic Gaussian monocycle $w_n(t) = \frac{d^n}{dt^n}(e^{-2\pi(t/t_p)^2})$, where t_p is a parameter that controls the pulse width. Besides the ease of mathematical modeling, these pulses provide two degrees of freedom that aid in coping with a given spectral mask, the pulse order, *n*, and t_p. Note that t_p determines the bandwidth of the pulse, and n corresponds to the shift in the central frequency of the spectrum [17]. Modified Hermite Pulses (MHP) have

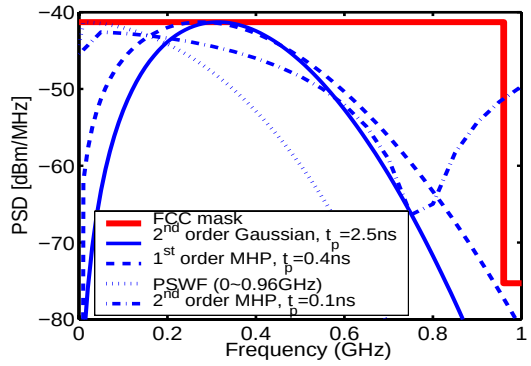

3(a)

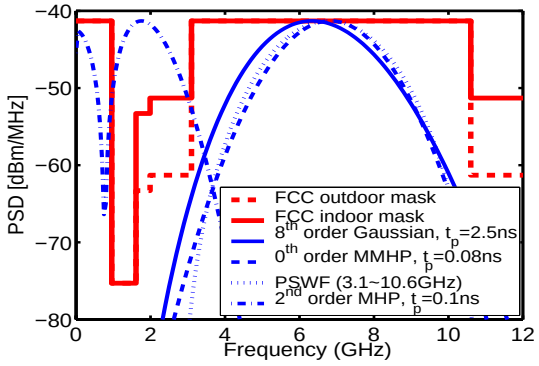

3(b)

Figure 3. PSD of pulses that satisfy the FCC spectral masks and of 2nd order MHP, (a) 0~0.96GHz band (b) 3.1~10.6GHz band.

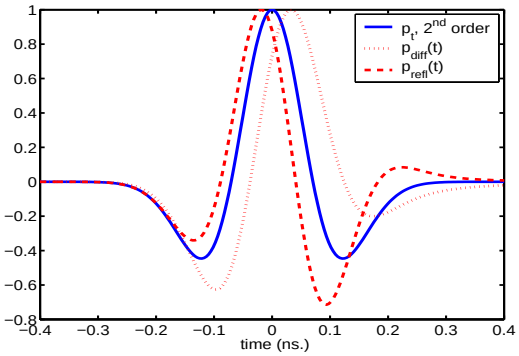

4(a)

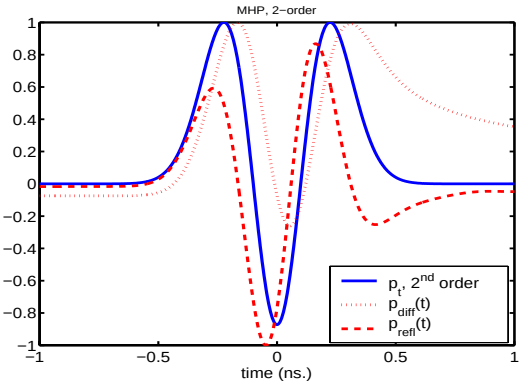

4(b)

Figure 4. Diffracted and reflected (small reflector) pulses with normalized amplitude: (a) 2nd order Gaussian monocycle, t_p=0.25ns, (b) 2nd order MHP, t_p=0.1ns.

also been proposed for UWB channels [18]. The advantage of MHP is the orthogonality between pulses of different orders that can be utilized in M-ary orthogonal modulation or to accommodate multiple users. The nth order MHP is defined by $\mathrm{MHP}_n(t) = (-1)^n \, e^{0.25(t/tp)^2} \frac{d^n}{dt^n} (e^{-0.5(t/tp)^2})$. The power spectrum density (PSD) of MHP for n>1 contains multiple lobes with the band of spectral occupancy from very low frequency to a few GHz [20]. Therefore, it is not straightforward for MHP to cope with the FCC spectrum mask [1]. To remedy this problem, Modulated Modified Hermite Pulse (MMHP) [20] can be employed. For generating MMHP, the corresponding MHP is multiplied by a cosine wave of frequency f_c. The value of f_c is usually chosen to be 6.85GHz, which is the central frequency of the 3.1~10.6GHz band of the FCC mask. Finally, Prolate Spheroidal wave function based pulses (PSWF) were investigated in [19]. It is straightforward to cope with a given frequency spectrum mask using PSFP, while the associated shortcoming is they have to be generated numerically and do not have the closed-form expression.

Within these pulse families, there are multiple choices of UWB pulses that satisfy the FCC spectral masks. As examples, the PSD of some pulses that satisfy both the indoor and outdoor FCC spectral masks is given in Fig. 3 along with the FCC masks (note that the two masks are identical in Fig. 3(a)). We also include the PSD for the 2nd order MHP pulse. The comparison in the time domain waveforms reveals that the pulses that fit the 0~0.96GHz band (Fig. 3(a)) are much wider than those that fit the 3.1~10.6GHz band (Fig. 3(b)), and all pulses that fit the same frequency band have comparable pulse widths. Moreover, the pulse waveforms of the three pulses that fit the 3.1~10.6GHz band are very similar, although they belong to different pulse families.

We employ the paths 1 and 3 in Fig. 1 with frequency responses shown in Fig. 2 to investigate the effect of diffraction and reflection by small reflector on these families of pulses. (The same qualitative conclusions were obtained for other paths with these propagation mechanisms). Fig. 4 illustrates the received pulse waveforms with normalized amplitude when the Gaussian monocycle and MHP, both of order 2, are transmitted (note that the distortion results do not depend on the pulse width t_p). We denote the received pulse waveform associated with the diffraction path and the reflection path as $p_{diff}(t)$ and $p_{refl}(t)$, respectively. We have found that while all pulses are distorted by these propagation mechanisms, the distortion is particularly dramatic for the diffracted MHP pulses of all orders. Note that the PSD of the MHP pulses is significant for very low frequencies (Fig. 3(a)) where the response of the diffracted path varies the most (see Fig. 2(a)), while the PSD of the Gaussian monocycle occupies relatively "flat"

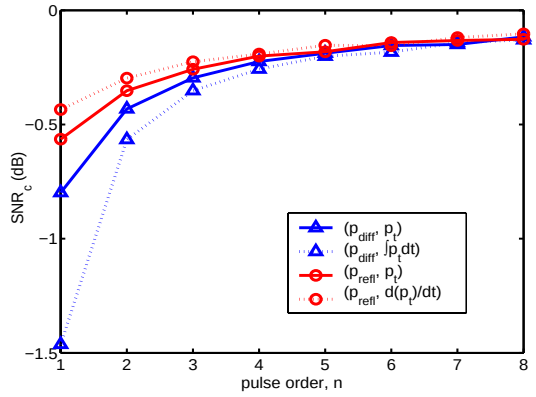

5(a)

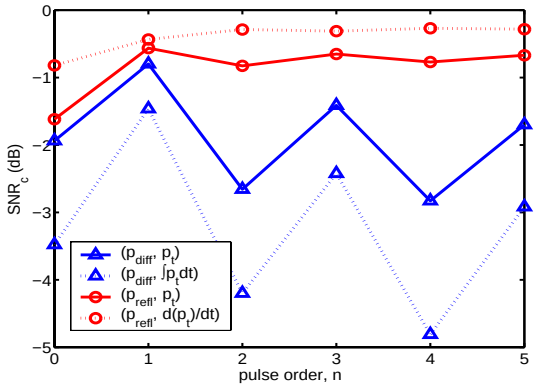

5(b)

Figure 5. SNR capture, (a) Gaussian monocycle, t_p=0.25ns, (b) MHP (t_p=0.1ns) and MMHP (t_p=0.1ns, f_c=6.85GHz).

region of the diffracted channel frequency response (recall that its amplitude resembles $H(f)=1/\sqrt{f}$). In addition, observe in Fig. 4(b) that the diffracted 2nd order MHP has much wider tail than the transmit pulse. The latter effect is due to the similarity of the diffracted channel to the integrator. The integral of the 2nd order MHP is not zero (its PSD is significant at dc), and thus diffraction causes the dispersion of the tail of the received pulse. In fact, all even-order MHP pulses and the PSWF pulse with PSD shown in Fig. 3(a) contain dc component, and experience similar dispersion. This pulse widening can cause interference in the receiver and reduce the data rate. Moreover, these pulses cannot be used in practice directly due to poor antenna radiating efficiency for very low frequencies [23]. However, their properties are of interest since they give rise to modulated waveforms with potentially low complexity receiver implementation that involves filtering of the original pulse situated at dc [24]. We also note that the received pulses of the reflected signals for all investigated pulses are also visibly distorted, but retain general shape characteristics of the transmitted pulses. In addition to the distortion, we observe the shift of the peak of the pulse that is related to the approximately linear phase of the frequency response.

In Fig. 5, we plot the SNR capture (3) that corresponds to the peak correlation (2), between the distorted received pulses and several suboptimal correlation templates for the diffracted path 1 (with response p_{diff}) and reflected path 3 (p_{refl}) in Fig. 1,2. In all cases, the transmit pulse is utilized as one of the templates. The integral $\int p_t(t)dt$ and the derivative $\frac{dp_t(t)}{dt}$ of the transmit pulse were employed as templates for the diffracted and the reflected cases, respectively, since these templates are easy to generate and produce good results. For the Gaussian monocycles, all template choices for n>1 result in less than 1 dB loss due to template mismatch. Note that the shift $\tau - \hat{\tau}$ is within 20% of the pulse width for all cases shown in the figures.

While the results for the MHP pulses are similar to those in Fig. 5(a) for the reflected path, our suboptimal correlation templates (the transmit pulse and the integrator) do not yield satisfying results for the diffracted MHP pulses, especially for the MHP of even orders due to the tail dispersion discussed above. Fig. 5(b) illustrates the comparison of the SNR_c between the MHP and the MMHP when the transmit pulse shape is used as template. The high-frequency carrier of the MMHP removes the dc component and spectral shaping that is beneficial for the diffracted channel as discussed above. Therefore, MMHP results in much higher peak cross-correlations than MHP. Similarly, the PSWF pulses in the higher band (Fig. 3(b)) has much better SNR_c than the PSWF pulse in the lower band (Fig. 3(a)).

From these results, we conclude that when MMHP, PSWF in the 3.1~10.6GHz band and Gaussian monocycles are used as transmit pulses, the transmit pulse shape represents near-optimal template for both diffracted and reflected single-path conditions, resulting in SNR_c within 1dB of the ideal template. This conclusion greatly simplifies the receiver design for channels with distortion, since accurate per-path channel response estimation is not required. Thus, these transmit pulses are 'robust' for outdoor UWB channels. This conclusion is consistent with the investigation of distortion due to penetration through various materials for pulses in the 3.1~10.6GHz band [10]. On the other hand, our results indicate that for certain pulses (e.g. MHP or PSWF in Fig. 3(a)), more accurate template design is required to obtain high energy capture.

IV. PROPAGATION GAIN AND IMPLICATIONS FOR ADAPTIVE TRANSMISSION

It is well known that shadowing, obstructions, etc. can significantly attenuate received signal power. This propagation loss is referred to as large-scale fading and affects all frequency components of conventional narrowband and spread spectrum systems similarly.

However, in the UWB channel, the received power is frequency-dependent, as illustrated by the following comparison. Define the propagation gain (PG) as the ratio of the received and the transmitted signal energies:

$$\mathrm{PG}\,(p_t) = \int_{-\infty}^{\infty} p_r^2(t)\mathrm{d}(t) \Big/ \int_{-\infty}^{\infty} p_t^2(t)\mathrm{d}(t). \qquad (4)$$

Note that this definition does not include the SNR capture (3) (received energy loss) due to the template mismatch, while the free space path loss due to the distance between the transmitter and receiver is included and the energy of the transmit pulse is measured at 1m (LOS) from the Tx antenna [21].

While most of the research on impulse radio to date has focused on the utilization of the 3.1~10.6 GHz band of the FCC mask, this spectrum allocation can potentially result in substantial performance degradation. For example, the loss due to diffraction is much lower in the 0~0.96GHz band since diffraction attenuates higher frequencies. In Fig. 6, the PG (4) is compared for the UWB pulses shown in Fig. 3 that reside in two different bands of the FCC mask as the receiver moves along the horizontal line A (see Fig. 1) from the shadowed area to the LOS area, and the reflector is not present. While all pulses become weaker as the receiver advances deeper into the shadowed region, the loss for the pulses in the 3.1~10.6GHz band is at least 13dB greater than for the pulses in the lower frequency band. The PSWF is about 5dB stronger in diffraction than the other two 'low frequency' pulses, but this pulse is not feasible in practice due to its dc component.

Similar comparison in [28] reveals that the propagation gain of the reflected signal (path 3 in Fig. 1) decreases linearly with the logarithm of the size of the reflector for sufficiently small reflector sizes. Above certain threshold (that decreases with the wavelength of the transmitted signal), the received signal does not experience loss due to reflection. For small reflectors, the pulses in the lower band experience about 13 dB loss relative to the pulses in the higher band. The insight into the 13dB gap between pulses in the two bands for both diffraction and reflection can be obtained by the examining the channel responses at the 'mode frequencies' $f_m^{\,l}$ and $f_m^{\,u}$ (corresponding to the peak of the pulse PSD) for the lower and upper bands, respectively. For the 2nd order Gaussian monocycle in Fig. 3(a), $f_m^{\,l}$=0.34GHz, while the 8th order Gaussian monocycle in Fig. 3(b) has $f_m^{\,u}$=6.5GHz. Using the approximations $1/\sqrt{f}$ and $\sqrt{f}$ of the diffracted and reflected channel amplitude responses, respectively, the ratio of the gains at the lower and upper mode frequencies is $(\sqrt{f_m^{\,u}}/\sqrt{f_m^{\,l}})^2 \approx 12.8$dB for the diffracted path, and $(\sqrt{f_m^{\,l}}/\sqrt{f_m^{\,u}})^2 \approx -12.8$dB for the reflection by small reflector.

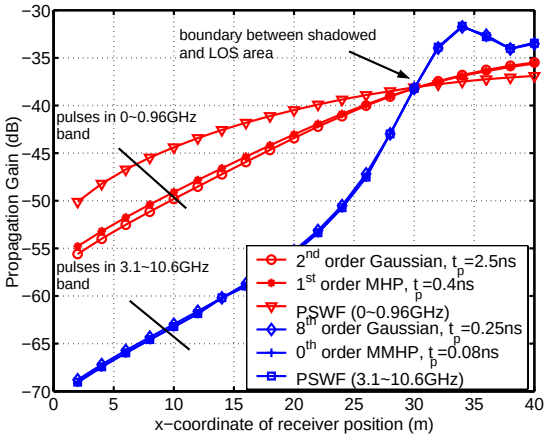

Figure 6. Propagation gain of pulses in Fig. 3 as the receiver moves along line A (see Fig. 1), the y-coordinate is 20, fixed, reflector is not presented.

Using the evaluation of the PG for different scenarios [28], it is observed that in the absence of LOS and large reflectors, either diffraction or reflection by a small reflector can be the dominant propagation mechanisms. For example, propagation into a canyon-like street can be dominated by diffraction. When a small reflector such as a sign or lamp-post is within LOS of both the transmitter and the receiver located in the canyon-like street, it can reflect energy into the street, and will likely be the dominant signal provider for part of that street. A similar situation is found for a tunnel [28].

Finally, we discuss the potential for adaptive transmission that that utilizes different bands of the UWB spectrum as a function of the dominant propagation mechanism. These signaling methods are motivated by the large gap in the PG for pulses in two different bands of the FCC mask. Of course, it is well known that lower frequencies propagate better in the presence of obstacles [21]. However, our novel physics-based study provides quantitative comparison of distortion and channel gains required for the development and verification of the proposed adaptive transmission schemes. In particular, assuming an ideal single-path received signal affected by either LOS of diffraction, a simple adaptive signaling method is to utilize the 8th order Gaussian monocycle in LOS, but to switch to the 2nd order Gaussian monocycle when the receiver is in the shadow. The receiver has to send the feedback signal to the transmitter to switch pulses when the appropriate power threshold is detected. This approach can be viewed as a variable rate adaptive transmission method, since utilization of the wider pulse in the lower band would result in decreased transmission rate for practical modulation techniques relative to the case when the narrower pulse in the higher band is employed [3, 8]. In addition to improved bandwidth and power efficiency relative to the conventional techniques that utilize fixed pulses in the higher band, the proposed

adaptive approach relaxes the stringent timing requirements of UWB impulse radio systems and improves timing estimation due to longer duration of the lower band pulse [25-27]. This is especially beneficial for degraded channel conditions when diffraction is dominant.

Of course, the single path model is greatly simplified. Extension of the model to multipath channels, where each path might experience per-path distortion specific to its propagation mechanism, and identification of dominant propagation conditions for this model is required to test the effectiveness of the proposed adaptive signaling techniques. The key feature of the proposed adaptive transmission method is the ability to switch between various bands depending on propagation conditions. This adaptive strategy can be applied to all UWB systems [3-6] to improve the transmission bandwidth and power efficiency.

V. CONCLUSIONS

A novel UWB physical model was developed and used to investigate per-path distortion and robust template design for single path channel model in dominant outdoor propagation conditions. It was demonstrated that while shadowing and reflection by small reflector cause significant frequency-dependent distortion, a simple template given by the transmit pulse shape captures most of the received energy for several popular UWB pulses, e.g. Gaussian monocycles and MMHP pulses. Some pulses that require more accurate channel-dependent template design were identified. Finally, we have quantified the frequency-dependent propagation gain for channels with per-path distortion and its implication on UWB adaptive transmission design.

REFERENCES

[1] Federal Communications Commission, "First Report and Order, Revision of Part 15 of the Commission's Rules Regarding Ultra Wideband Transmission Systems," ET Docket 98-153, February 14, 2002.

[2] C. J. Le Martret and G. B. Giannakis, "All-digital impulse radio for MUI/ISI-resilient transmissions through frequency-selective multipath channels," Proc. *MILCOM*, vol. 2, pp. 655–659, Oct 2000.

[3] R.A. Scholtz, "Multiple Access with Time Hopping Impulse Modulation," invited paper, *Proc. MILCOM'93*, Dec. 1993, pp. 447-450.

[4] B. R. Vojcic and R. L. Pickholtz, "Direct sequence code division multiple access for ultrawide bandwidth impulse radio," *Proc. MILCOM'03*, Vol. 2, pp 898-902, 2003.

[5] O.S. Shin, S.S. Ghassemzadeh, L.J. Greenstein, V. Tarokh, "Performance Evaluation of MB-OFDM and DS-UWB Systems for Wireless Personal Area Networks", *Proc. ICU'05*, September 2005.

[6] J. Balakrishnan, A. Batra, and A. Dabak, "A multi-band OFDM system for UWB communication," *Proc. UWBST'03*, Nov. 2003, pp. 354–358.

[7] "IEEE 802.15 high data rate alternative PHY task group 3a for wireless personal area networks", http://www.ieee8o2.org/15/pub/TG3a.html.

[8] M. Z. Win and R. A. Scholtz, "Impulse radio: how it works," *IEEE Commun. Lett.*, vol. 2, no. 2, pp. 36–38, 1998.

[9] R. C. Qiu, "A Study of the Ultra-wideband wireless propagation channel and optimum UWB receiver design," *IEEE JSAC,* Vol. 20, No. 9, pp. 1628-1637, Dec. 2002.

[10] R.D. Wilson, R. A. Scholtz, "Template Estimation in Ultra-Wideband Radio," *Signals, Systems and Computers, Conference Record of the Thirty-Seventh Asilomar Conference on,* Nov. 2003.

[11] A. F. Molisch *et al.* "IEEE 802.15.4a channel model – final report," Tech. Rep. Document IEEE 802.15-04-0662-02-004a, 2005.

[12] G. Durgin, T. S. Rappaport, H. Xu, "Measurements and models for radio path loss and penetration loss in and around homes and trees at 5.85 GHz", *IEEE Trans. On Commun.*,vol. 46, No. 11, Nov. 1998.

[13] R.C. Qiu, Physics-based Generalized Multipath Model and Optimum Receiver Structure, book chapter, *Design and Analysis of Wireless Networks*, Nova Science Publishers, 2004.

[14] H. Hallen, A. Duel-Hallen, S. Hu, T.S. Yang, M. Lei, "A Physical Model for Wireless Channels to Provide Insights for Long Range Prediction", in *Proc. of MILCOM'02*, Oct. 7-10, 2002.

[15] R.D. Guenther, Modern Optics, New York: Wiley, 1990

[16] L.B. Felsen and N. Marcuvitz, Radiation and Scattering of Waves, Prentice-Hall, 1973.

[17] J. Zhang, T. D. Abhayapala and R. A. Kennedy, "Performance of Ultra-wideband Correlator Receiver Using Gaussian Monocycles," in *Proc. IEEE ICC 2003*.

[18] L. B. Michael, M. Ghavami and R. Kohno, "Multiple pulse generator for ultra-wideband communication using Hermite polynomial based orthogonal pulses," *Proc. UWBST'02*, May 20-23, 2002, pp. 47-51.

[19] B. Parr, B. Cho, K. Wallance and Z. Ding, "A novel ultra-wideband pulse design algorithm*," IEEE Commun. Lett.*, vol. 7, pp.219-221, May 2003.

[20] H. Harada, K. Ikemoto and R. Kohno, "Modulation and hopping using modified Hermite pulses for UWB communications," in *Proc. of joint UWBST&IWUWBS'04*, Kyoto, Japan, May 2004.

[21] T. S. Rappaport, Wireless Communications, Prentice-Hall, 1996.

[22] R. C. Qiu, "Time/frequency dispersion of digital transmission media: Wideband wireless channel model, chiral optical fiber, and superconducting MMIC," Ph.D. Dissertation, Ploytechnic University, Jan. 1996.

[23] X. Chen and S. Kiaei, "Monocycle shapes for ultra wideband system", *Proc. ISCAS'02*, vol.1, pp.I597-I600, 2002.

[24] M. Verhelst and W. Dehaene, "System design of an ultra-low power, low data rate, pulsed UWB receiver in the 0-960MHz band", in proc. IEEE ICC 2005, Seoul, Korea

[25] D. Rowe et al, "A Si/SiGe HBT timing generator IC for high-bandwidth impulse radio applications," in *Proc. IEEE 1999 Custom Integrated Circuits Conf.*, 1999, pp. 221-224.

[26] D. Kelly, S. Reinhardt, R. Stanley, and M. Einhorn, "PulsON second generation timing chip: enabling UWB through precise timing," *Proc. UWBST'02*, pp. 117-122, 2002.

[27] V. Lottici and U. Mengali, "Channel estimation for ultra-wideband communications," *IEEE JSAC*, vol. 20, no. 9, pp. 1638-1645, Dec. 2002.

[28] L. Ma, "Investigation of transmission, propagation and detection of UWB pulses using physical modeling," Ph.D. Dissertation, North Carolina State University, Dec. 2006.